Preprints of the 21st IFAC World Congress (Virtual)
Berlin, Germany, July 12-17, 2020

Active Power Regulation of a Storage Power Plant (SPP) with Voltage Angle Control as Ancillary Service

Paul Gerdun, **Nayeemuddin Ahmed**, **Harald Weber**

Electrical Energy Supply (EEV), University of Rostock,
Rostock 18059, Germany
E-mail: (paul.gerdun, nayeemuddin.ahmed,
harald.weber)@uni-rostock.de

Abstract:
Electrical Energy Storage (EES) plays an increasingly important role to balance the intermittent power generation and demand, thus ensuring a more reliable network. An example of such an EES is the Storage Power Plant (SPP). It has been proved in previous studies that the SPP not only improves the power supply security but also reduces redispatch costs. However, its protection features against overcurrent and exceeding of its generation limit or storage capacity have not been discussed yet. In reality, such events can occur, leading to unexpected grid failures as a worst case scenario. Thus, the aim of this paper is to exhibit the behavior of a controller model which has been implemented in the SPP to protect the power plant during such situations. In this investigation, once the SPP's active power output is about to surpass its limit, the power plant automatically switches to a different mode of operation at the threshold value to prevent this from happening. In this manner, the SPP can protect itself autonomously and also helps to create a more robust system.

Keywords: Energy storage, Power System Stability, Control system design, Redispatch, Security

1. INTRODUCTION

Currently, 14.8% of Germany's gross final energy consumption (approximately 2500 TWh) originates from renewable energy sources (RES) (International Energy Agency (2016)). The aim of the EU 2020 energy strategy is to raise this share to 18% with future targets projecting it to be around 60% by the year 2050 (Weber et al. (2006); European Commission Directorate-General for Energy (2011); VGB POWERTECH Facts and Figures (2018); Energiewende (2015)). Such high penetration of renewable energy (wind and solar), although necessary, introduces additional challenges in ensuring stability and reliability of the electrical grid. The ever increasing feed in from these RES leads to higher frequency fluctuations, presence of harmonics as well as increased forecast errors due to their intermittent nature (Liang (2016)).

The difference between the varying electrical energy generation from RES and consumption by loads leads to an energy deficit or surplus in the grid. At present, conventional power plants (CPP) have to compensate for this disparity. However, in the future, the number of these CPP, especially coal fired power plants, will decrease significantly to fulfill energy sector targets (German Institute for Economic Research (DIW Berlin) (2019)). Thus, Electrical Energy Storage (EES) systems are regarded as viable alternatives to compensate for the intermittent and decentralized RES, so that the network demand can be met at all times.

Depending on its principle a storage type has different advantages and disadvantages. Flywheels and Supercapacitors have high charge and discharge rates, but, due to their sizes, are impractical long-term energy storages (Hadjipaschalis et al. (2009)). In comparison to supercapacitors, battery energy storages have a higher energy density but a much slower response (Dunn et al. (2011)). Hydrogen storages can be used to store large magnitudes of energy but due to the electrochemical reactions via a fuel cell or electrolyser their response is even slower. A combination of these elements, though, will not only compensate for the shortcomings of these individual storage types but also assist in exploiting their advantages. Hence, such an interconnected system is presented in this paper, called Storage Power Plant (SPP).

In the future, with most of the traditional power plants (possessing rotating masses) being replaced by an increasing number of converters in the grid, a frequency independent governing principle can be used. Such a form of ancillary service is called Voltage Angle Control (Weber et al. (2018a,b,c)). The SPP, to be deemed truly feasible, has to be able to protect itself from damage caused by exceeding its minimal and maximal active power rating. Thus, the goal of this paper is to investigate the dynamic behaviour of the SPP under such situations.

⋆ Research project - "Netz-Stabil", financed by the European Social Fund (**ESF/14-BM-A55-0025/16**)

2. TEST ELECTRICAL NETWORK

The test bench for the investigations is shown in Fig. 1. The network consists of 25 equidistant nodes, each connected to either a power plant or a load. The nodes are interconnected via transmission lines, each 250 km long and at a voltage level of 110 kV. The line impedances are equal in magnitude with a resistance to reactance ratio of 0.1. Such a squared grid is used to easily highlight the principles of power production of the four different kinds of power plants present in the test bench. This will become more apparent once Fig. 5 is analyzed.

There are eleven power plants, of which five are slack SPPs (S), i.e. converters at terminals where the voltage magnitude ($|V|$) and angle (ϕ_u) are kept constant. Out of the other six, four represent wind power plants (W), while the other two each denote a conventional hydroelectric

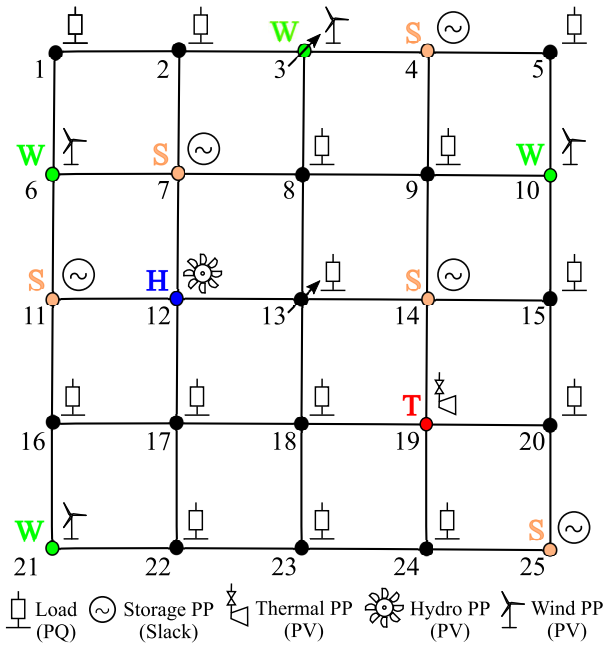

Fig. 1. 25 node electrical network

Table 1. Initial working points of the different power plants and loads

Type	No.	Power per PP (MW)	Total power (MW)
Thermal power plant	1	23.516	23.516
Hydro power plant	1	23.516	23.516
Wind power plant	4	23.516	94.064
Storage power plant	5	0	0
Total generation	-	-	**141.1**
Load	14	10	140
Losses	-	-	1.10
Total consumption	-	-	**141.1**

(H) and a coal fired thermal (T) power plant. The CPPs are represented by PV terminals, where the active power (P) and voltage magnitude ($|V|$) are controlled. The four wind power plants (WPPs) and remaining 14 nodes, each housing a load, are represented by PQ terminals where the active (P) and reactive power (Q) consumed are known.

The network modeling and RMS simulations are performed in the software DIgSILENT PowerFactory with the base power value of the per-unit-system as 10 MVA. The initial load flow setpoints for the different power plants are summarized in Table 1. Each load also consumes 3.3 MVAR of reactive power which is supplied by the power plants. Unfortunately, the reactive power results and control methods are not included in this paper due to space constraints.

3. INTERNAL SPP STRUCTURE

As seen in Fig. 2, the SPP consists of three main storages; the supercapacitor, battery and hydrogen storage. These storages have different energy capacities and are responsible for providing inertial, primary and secondary control response respectively. There are DC-DC convert-

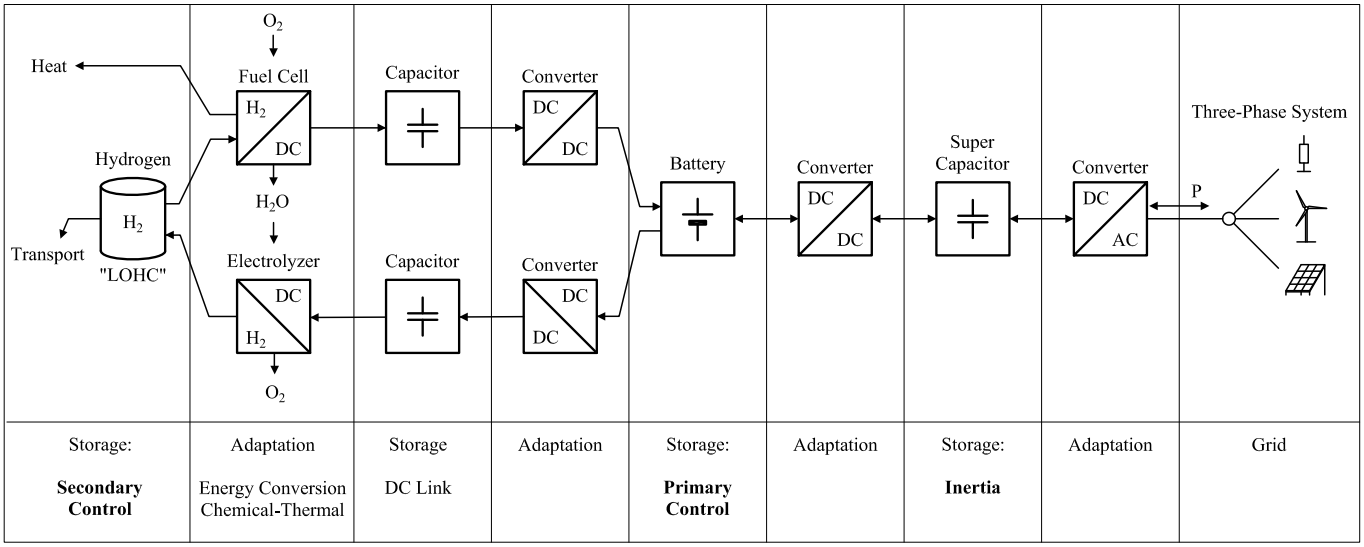

Fig. 2. Working principle of the internal components of a storage power plant (SPP)

ers which control the power flow between the storages. All components operate in DC mode. Hence, the power plant uses a DC-AC converter for grid connection. The SPP structure used in the simulation software, models the control scheme of the DC-DC converters which govern the power flow between the SPP storage components.

The first storage, i.e. the supercapacitor, is directly connected to the DC-AC grid converter. In case of a network disturbance, it immediately supplies inertial power to the grid or stores it from the grid. It can instantaneously charge and discharge with high power and additionally has an almost infinite lifetime because of its electrostatic storage principal. These properties make it ideal for its task of providing inertial control. Hence, its behavior is analogous to the rotating mass in a turbine shaft of a conventional thermal power plant (TPP).

The second storage, i.e. the battery, connected in parallel to the supercapacitor, supplies or stores primary control power, in order to compensate for the low power density of the supercapacitor. This process is controlled by the DC-DC converter between these two components. In contrast to a supercapacitor, the battery is optimally suited for the purpose of providing primary control power. This is due to its electrochemical energy storage principle which allows it to possess a higher energy storage density compared to a supercapacitor and a preferably lower charging and discharging gradient, to improve its lifetime. Thereby, it represents the equivalent of the steam boiler in a conventional TPP.

As the third main storage, the hydrogen storage is responsible for supplying secondary control power, similar to the coal storage in a coal fired TPP. Additionally, it can store secondary control power. Depending on the power flow direction, either a fuel cell or an electrolyser is used to empty or refill the hydrogen storage. The power flow for each of these cases is controlled by the DC-DC converter

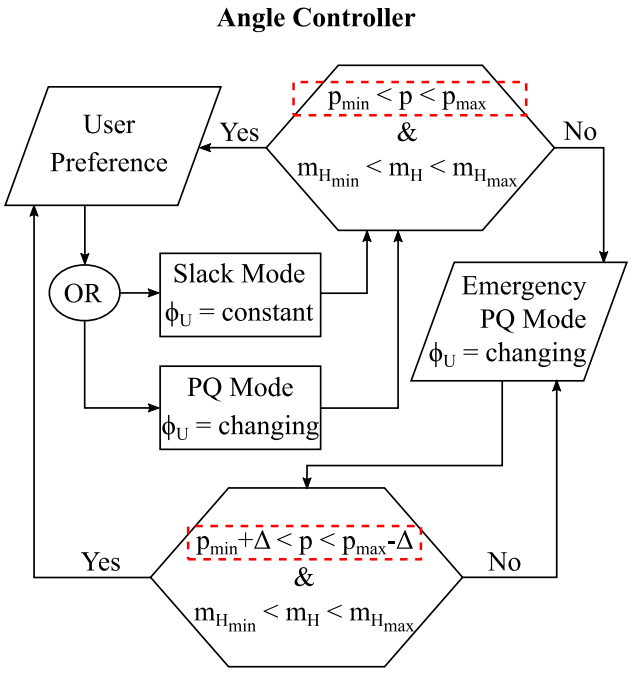

Fig. 3. Functional overview of the SPP angle controller

in the respective paths between the hydrogen storage and the battery. Each of these two DC-DC converters possesses a DC link buffer storage. The behavior of these capacitors is analogous to the steam boiler pipe wall in a TPP.

While utilizing the hydrogen storage, the fuel cell generates electrical energy from the chemical reaction between stored hydrogen (H_2) and external oxygen (O_2). One by-product of this reaction is thermal energy which can be used for district heating. Another product is dihydrogen monoxide (H_2O). In case of a reversed power flow, the H_2O can in turn be used as the electrolyte to generate hydrogen as well as oxygen as a by-product. The hydrogen can then be stored in a Liquid Organic Hydrogen Carrier (LOHC) system. Such a system enables safe, easy storage and transportation of hydrogen at a high energy density under ambient conditions, using the currently available infrastructure (Teichmann et al. (2011)). In addition to being used for electrical power generation in the SPP, the stored hydrogen can also be utilized in other applications, for example in automobiles.

4. ANGLE CONTROLLER OF THE SPP

The active power of the SPP needs to be controlled for two reasons:

(1) Delivering controlled power to the grid
(2) Protecting the power plant from overcurrent and voltage fluctuations beyond permissible limits

These criteria are satisfied by the angle controller of the SPP, which is able to control the active power generation of the power plant via the voltage angle (ϕ_U) at its connection terminals. As described in the process flow diagram in Fig. 3, once the active power and stored hydrogen mass are within the boundaries, the SPP can be run by the operator in either Slack or PQ mode. This choice is also influenced by the power demand on the electrical network.

In slack mode, the SPP keeps its voltage angle constant (grid former) and uses the difference to the voltage angles of the surrounding load nodes to produce more power. This is more evident in the analysis of Fig. 5. If the plant operator opts for a constant active power generation from the SPP, then it's switched to PQ mode to allow the converter system function instead as a grid follower. If either the power output or the stored hydrogen mass surpasses the implemented margins, the SPP automatically switches to Emergency PQ mode as a protective measure to lower its power output. Under such circumstances, the operator can also shut down the power plant, if necessary. While in Emergency PQ mode, the SPP will continue to remain in this state, till its stored hydrogen mass returns to acceptable levels and its power output is within its corresponding bounds which includes the hysteresis band (Δ). Then, the SPP can once again function in either mode.

5. RESULTS AND OBSERVATION

To analyze the dynamic transition of the SPP between its modes of operation at its maximum generation limit, the following investigation is performed on the 25 node network, shown in Fig 1. A ramp increase is applied to the

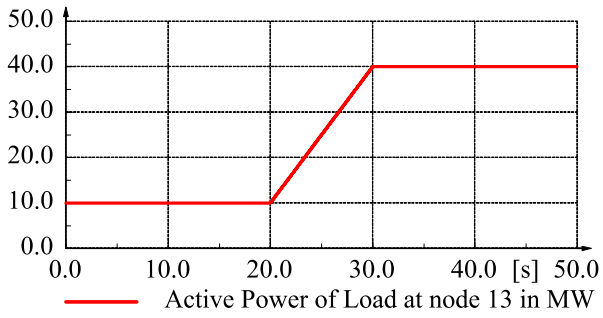

Fig. 4. Ramp increase in the power consumption by the load at node 13

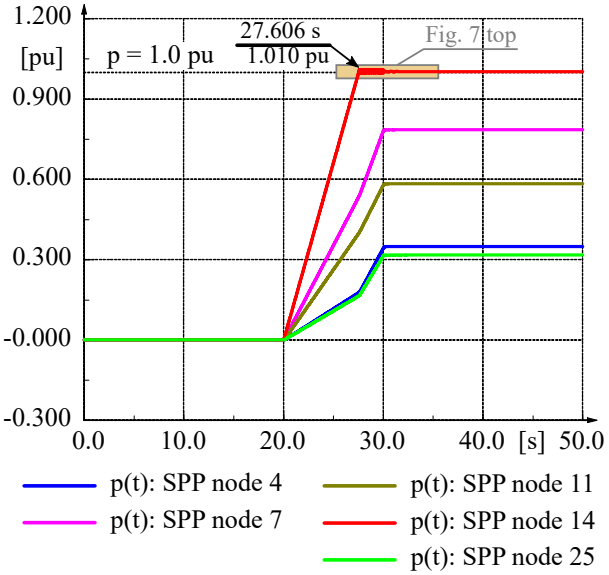

Fig. 5. Increase in active power generation of all the SPPs in response to the initial ramp increase in load demand at node 13

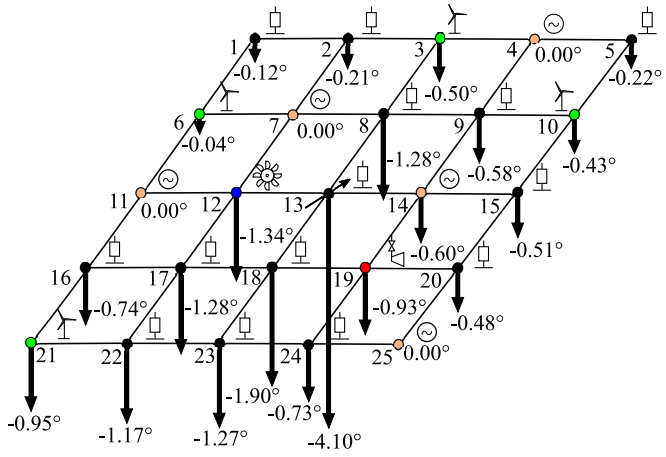

Fig. 6. Changes in nodal voltage angles due to the ramp increase in power demand at node 13

active power demand in the load at node 13, causing the power consumption to increase from 10 MW to 40 MW between 20 s and 30 s.

In response, the SPPs in the grid, initially in slack mode, increase their active power output with the one closest to the changing load at node 13 producing more power

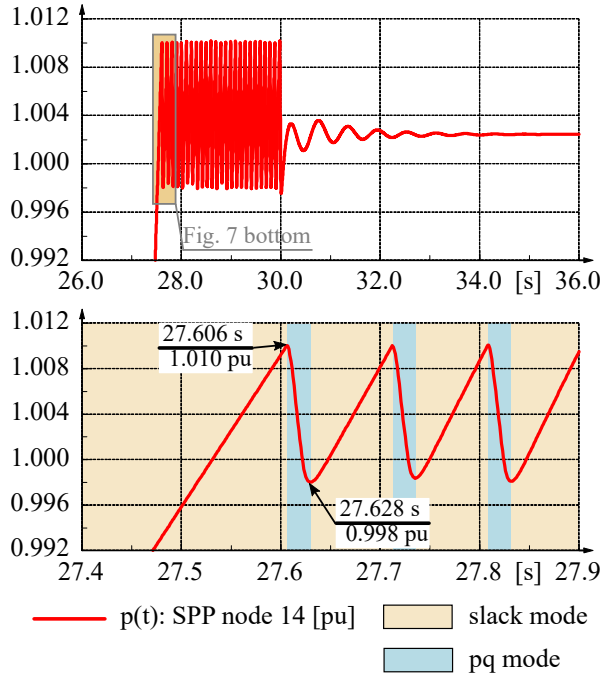

Fig. 7. Behaviour of SPP at node 14 upon reaching its maximum power limit

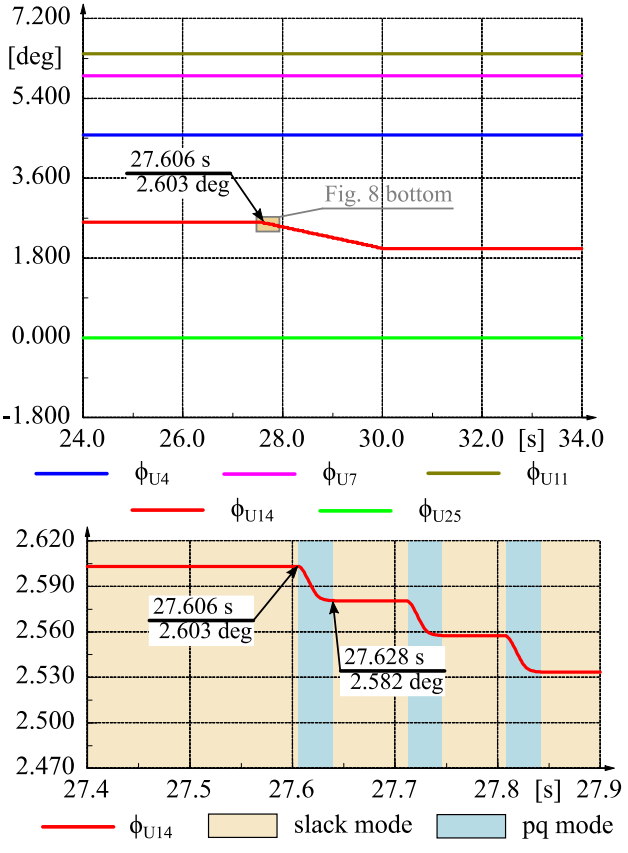

Fig. 8. Voltage angles of the SPPs during load ramp (top) and that of the SPP at node 14 upon reaching its maximum power limit(bottom)

than the others, shown in Fig. 5. The reason for this is the manner in which the voltage angles change at the nodes when there is a disturbance in the network. The

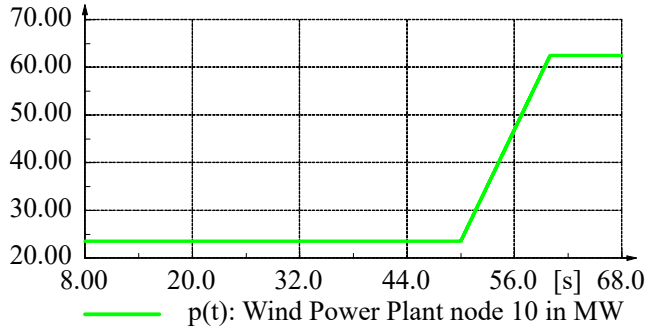

Fig. 9. Ramp increase in wind power at node 10

voltage angles change more for loads closer to load 13 and stay constant for slacks, as shown in Fig. 6. The resulting increase in the angles between these two enables the slacks near load node 13 to produce more active power. Hence, following a disturbance in a network governed by nodal voltage angle control, the power plants closer to the point of disturbance will provide greater ancillary services. As opposed to frequency control, this will allow the power plants further away to remain relatively undisturbed.

As the power demand keeps increasing, the SPP at node 14 reaches its maximum power limit (p_{max}) of 1.01 pu at 27.606 s, as shown in both Fig. 5 and the lower part of Fig. 7. Till this time, its voltage angle also remains constant at 2.603°, Fig. 8. To protect itself against further power increase, the SPP switches to Emergency PQ mode, allowing its voltage angle and power output to decrease. To compensate for this decrease in power production, the four other SPPs in the grid increase their rate of power generation to satisfy the total demand. Once the power output of the SPP at node 14 reduces beyond the threshold value including the hysteresis ($p_{max} - \Delta$) at 27.628 s, the danger is averted and the SPP switches back to slack mode to keep its voltage angle constant and increase its power output as the load ramp continues. This transition between slack and PQ mode repeats till the end of the ramp. After 30 s, the SPP at node 14 is again in slack mode. For the next couple of seconds there are some minor oscillations in the SPP output introduced by the Hydroelectric Power Plant (HPP) at node 12 due to its close proximity to the SPP and the changing load at node 13.

For the next investigation, a ramp increase is applied to the active power generation of the WPP at node 10. As a result, the power output at this node increases by 40 MW between the time duration of 50 s and 60 s, as shown in Fig. 9. At 50 s, all the SPPs are in slack mode after their response to the initial increase in demand. Following the onset of the increase in wind power, all the SPPs lower their power output according to their electrical proximity to WPP at node 10 due to voltage angle control. In this case, both the SPPs at nodes 4 and 14 are the closest and electrically equidistant from the WPP at node 10. Hence, both these SPPs reduce their power at the same rate, shown in Fig. 10. Since, the SPP at node 4 had a lower power output than the SPP at node 14 during the inception of the wind power ramp, it reaches the lower maximum power limit of -1.01 pu first at 58.012 s. During this time, the wind ramp is still continuing and the four other SPPs correspondingly start to reduce their power

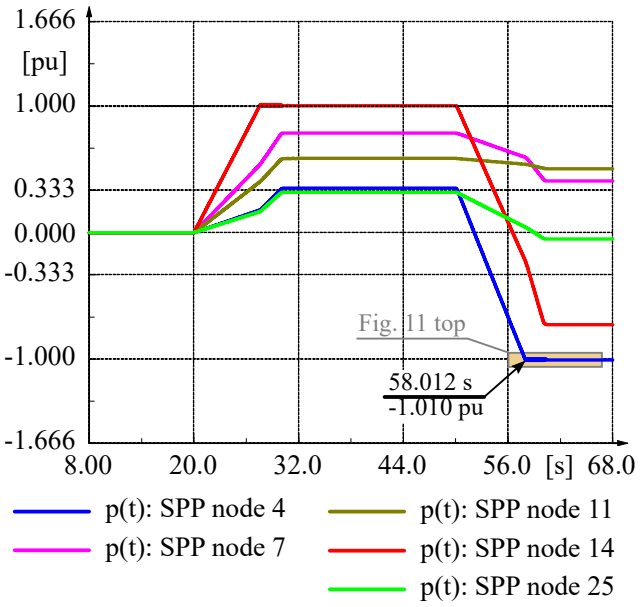

Fig. 10. Decrease in active power generation of all the SPPs in response to the increase in wind power at node 10

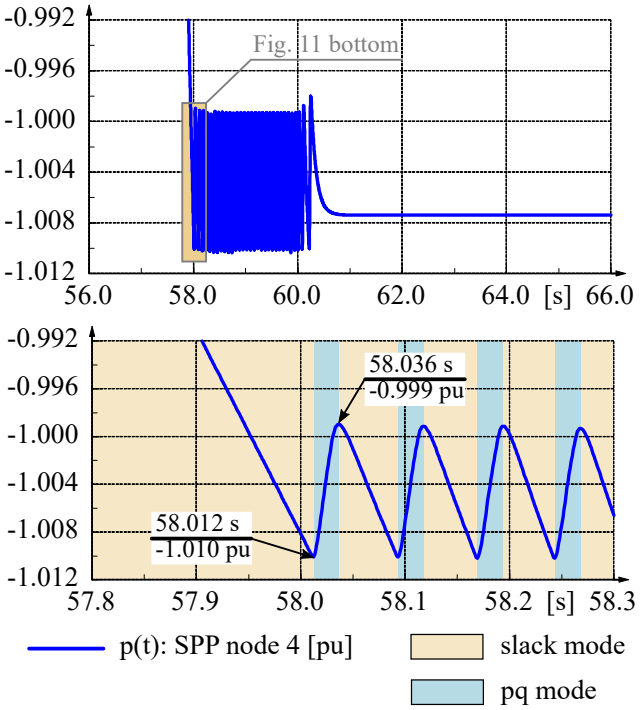

Fig. 11. Behaviour of SPP at node 4 upon reaching its minimum power limit

output at a faster rate with the SPP at node 14 doing the bulk of the work due to its proximity to node 10.

Upon reaching its lower output power limit, the SPP at node 4 switches to Emergency PQ mode, allowing its voltage angle and output power to increase, as shown in the Figs. 11-13. Once the power output increases above the lower threshold value including the hysteresis ($p_{min} + \Delta$) at 58.036 s, the SPP switches to slack mode once again to keep its voltage angle constant and reduce its power output as the wind ramp continues. This transition between slack and PQ mode is analogous to what was discussed in the

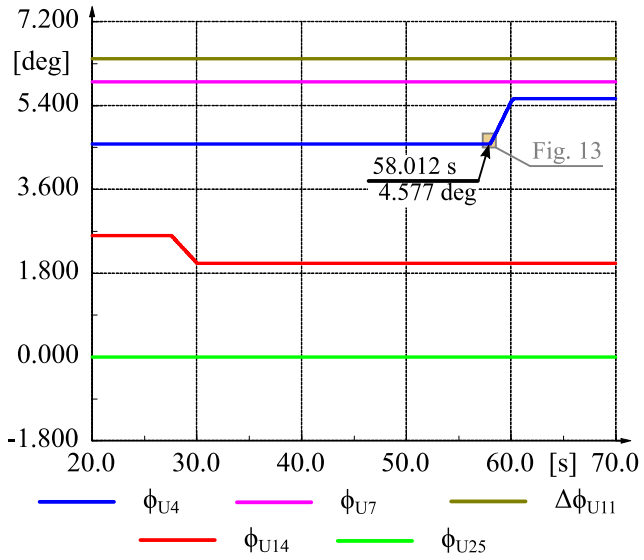

Fig. 12. Voltage angles of SPPs during wind ramp

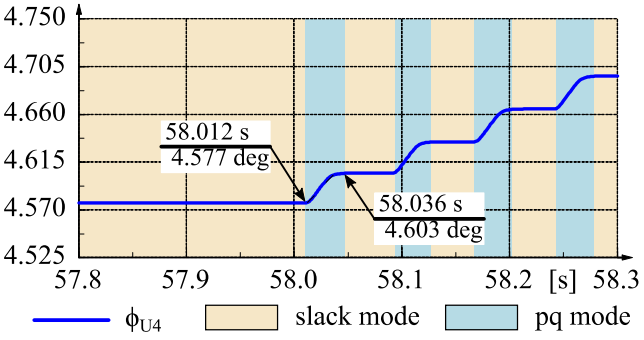

Fig. 13. Voltage angle of SPP at node 4 upon reaching its minimum power limit

first case. At the end of the ramp, the SPP at node 4 switches to slack mode, causing its voltage angle to be constant again. However, in this case, following the end of the ramp there are no oscillations in the power output of the SPP due to the HPP at node 12 owing to the comparatively larger electrical distance between the two as opposed to that between the SPP at node 14 and the HPP in the previous case.

6. CONCLUSION

This paper exhibits the autonomous response of the SPPs to protect themselves once their operational power limits are reached. To run preliminary tests and prove this concept, a 25 node network with multiple types of power plants was used as a test environment. In this network, disturbances were created by changing the load and generation causing different SPPs to reach their upper and lower power limits in separate investigations. Upon reaching the respective power thresholds, the SPPs switched from slack to Emergency PQ mode to always keep their power output within permissible limits. During this time, the other SPPs in the grid, which did not reach their operational limits, adjusted their power output to meet the load demand. Additional investigations need to be carried out to exhibit the consequences of this switching control in alternate grid configurations. The reactive power control schemes of the SPPs are also being investigated. In addition, further research will be required to estimate the total losses as well as the market compatibility of this novel system and hence prepare a quantitative comparative study in relation to the current power system.

ACKNOWLEDGEMENTS

This paper was made within the framework of the research project “Netz-Stabil” and financed by the European Social Fund (**ESF/14-BM-A55-0025/16**). It is part of the qualification program “Promotion of Young Scientists in Excellent Research Associations - Programme for Excellence in Research in Mecklenburg-Western Pomerania”.

REFERENCES

Dunn, B., Kamath, H., and Tarascon, J.M. (2011). Electrical energy storage for the grid: a battery of choices. *Science*, 334(6058), 928–935.

Energiewende (2015). The Energy of the Future, fifth energy transition monitoring report.

European Commission Directorate-General for Energy (2011). Energy 2020. URL `https://ec.europa.eu/energy/sites/ener/files/documents/2011_energy2020_en_0.pdf`.

German Institute for Economic Research (DIW Berlin) (2019). Phasing out Coal in the German Energy Sector. 45.

Hadjipaschalis, I., Poullikkas, A., and Efthimiou, V. (2009). Overview of current and future energy storage technologies for electric power applications. *Renewable and sustainable energy reviews*, 13(6-7), 1513–1522.

International Energy Agency (2016). IEA World Energy Balances. URL `https://www.iea.org/statistics?country=GERMANY&year=2016&category=Energy%20consumption&indicator=TFCbySource&mode=chart&dataTable=BALANCES`.

Liang, X. (2016). Emerging power quality challenges due to integration of renewable energy sources. *IEEE Transactions on Industry Applications*, 53(2), 855–866.

Teichmann, D., Arlt, W., Wasserscheid, P., and Freymann, R. (2011). A future energy supply based on liquid organic hydrogen carriers (LOHC). *Energy & Environmental Science*, 4(8), 2767–2773.

VGB POWERTECH Facts and Figures (2018). Electricity Generation.

Weber, H., Hamacher, T., and Haase, T. (2006). Influence of wind energy on the power station park and the grid. *IFAC Proceedings Volumes*, 39(7), 59–64.

Weber, H., Ahmed, N., and Baskar, P. (2018a). Nodal voltage angle control of power systems with renewable sources, storages and power electronic converters. In *2018 International Conference on Smart Energy Systems and Technologies (SEST)*, 1–6. IEEE.

Weber, H., Ahmed, N., and Baskar, P. (2018b). Power redispatch reduction with nodal voltage angle control in electrical energy supply systems. *IFAC-PapersOnLine*, 51(28), 576–581.

Weber, H., Baskar, P., and Ahmed, N. (2018c). Power system control with renewable sources, storages and power electronic converters. In *2018 IEEE International Conference on Industrial Technology (ICIT)*, 1–7. IEEE.